

General-purpose quantum circuit simulator with Projected Entangled-Pair States and the quantum supremacy frontier

Chu Guo,^{1,*} Yong Liu,^{2,*} Min Xiong,² Shichuan Xue,² Xiang Fu,² Anqi Huang,² Xiaogang Qiang,² Ping Xu,² Junhua Liu,^{3,4} Shenggen Zheng,⁵ He-Liang Huang,^{1,6,7} Mingtang Deng,² Dario Poletti,^{8,†} Wan-Su Bao,^{1,7,‡} and Junjie Wu^{2,§}

¹Henan Key Laboratory of Quantum Information and Cryptography, SSF IEU, Zhengzhou 450001, China

²Institute for Quantum Information & State Key Laboratory of High Performance Computing, College of Computer, National University of Defense Technology, Changsha 410073, China

³Information Systems Technology and Design, Singapore University of Technology and Design, 8 Somapah Road, 487372 Singapore

⁴Supremacy Future Technologies, Guangzhou 511340, China

⁵Center for Quantum Computing, Peng Cheng Laboratory, Shenzhen 518055, China

⁶Hefei National Laboratory for Physical Sciences at Microscale and Department of Modern Physics, University of Science and Technology of China, Hefei, Anhui 230026, China

⁷CAS Centre for Excellence and Synergetic Innovation Centre in Quantum Information and Quantum Physics, University of Science and Technology of China, Hefei, Anhui 230026, China

⁸Science and Math Cluster and EPD Pillar, Singapore University of Technology and Design, 8 Somapah Road, 487372 Singapore
(Dated: June 12, 2022)

Recent advances on quantum computing hardware have pushed quantum computing to the verge of quantum supremacy. Random quantum circuits are outstanding candidates to demonstrate quantum supremacy, which could be implemented on a quantum device that supports nearest-neighbour gate operations on a two-dimensional configuration. Here we show that using the Projected Entangled-Pair States algorithm, a tool to study two-dimensional strongly interacting many-body quantum systems, we can realize an effective general-purpose simulator of quantum algorithms. This technique allows to quantify precisely the memory usage and the time requirements of random quantum circuits, thus showing the frontier of quantum supremacy. With this approach we can compute the full wave-function of the system, from which single amplitudes can be sampled with unit fidelity. Applying this general quantum circuit simulator we measured amplitudes for a 7×7 lattice of qubits with depth $1 + 40 + 1$ and double-precision numbers in 31 minutes using less than 93 TB memory on the Tianhe-2 supercomputer.

Quantum computers offer the promise of efficiently solving certain problems that are intractable for classical computers, most famously factorizing large numbers [1–3]. With the rapid progress of various quantum systems towards Noisy Intermediate-Scale Quantum computing devices [4–11], we are now on the verge of *quantum supremacy* [12], i.e. demonstrating that an actual quantum computer has the ability to do a computation that no classical computers can tackle, an important milestone in the field of computer science. Various computations have been suggested to demonstrate quantum supremacy, such as BosonSampling [13, 14], the instantaneous quantum polynomial protocol [15, 16] and random quantum circuits (RQCs) [3, 17] which demand less physical resources and are easier to implement compared to, for instance, factorization. The central aspect for all these near-term supremacy proof-of-principle computations, which poses fundamental limitations to classical computations, is that the quantum states produced, and from which we wish to sample configurations, live in a Hilbert space that grows

exponentially with the system size.

In view of recent progresses in quantum computing hardware, in the following we focus on RQCs. They consist of a series of single and two-qubit gates which are applied to different qubits in a particular order. A group of commuting gates which can be applied simultaneously constitute one layer of the circuit, and the more groups of operations that do not commute, the *deeper* the calculation is. The qualification of random circuit comes from the fact that the single-qubit gates applied are chosen at random from a small set of them (for more details about the algorithm we implement see Appendix. A and [18]). RQCs have also stimulated the search for efficient classical algorithms which would show where exactly the limits of classical simulations are [17–25].

Except for the simulators which exactly represent the quantum state by storing the quantum state vector [19, 21], which are bounded by around 42 qubits, in general the memory required (space complexity \mathcal{C}^s) and the time needed (time complexity \mathcal{C}^t) by the quantum simulators mentioned above have not been shown explicitly. Hence, it is unclear what is the largest simulation that a modern supercomputer can possibly reach for RQCs. In [18] it is stated that the complexity scales exponentially with $\min(O(dL), O(N))$, for a N -qubit circuit with depth d and a minimum lateral size L . However an order of

*These authors contribute equally to this work.

†Electronic address: dario_poletti@sutd.edu.sg

‡Electronic address: bws@qiclab.cn

§Electronic address: junjiewu@nudt.edu.cn

magnitude estimate is not sufficient to have a clear evaluation of what is required for current and future quantum computers to demonstrate quantum supremacy.

In this work, we merge this line of research with that of many-body quantum physics where advanced tools have been developed to simulate strongly interacting quantum systems. In particular we present an efficient and generic quantum circuit simulator based on the Projected Entangled-Pair States (PEPS) algorithm [26–34], a type of tensor-network quantum states representation designed for two-dimensional lattices. Our PEPS based simulator is a general-purpose quantum circuit simulator for arbitrary quantum circuits: it stores the full quantum state exactly and it can be used to compute single amplitudes, observables, and also sequences of measurements, all with unit fidelity. We apply this simulator to study RQCs with depth $(1 + d + 1)$ where the '1's indicate the Hadamard gates applied to each site at the beginning and at the end of the calculations, while d is the number of non-commuting layers including controlled-Z (CZ) gates and single qubit gates applied to different sites. With our PEPS simulator we can precisely quantify the space and time complexity which clearly indicate where the quantum supremacy frontier is.

We demonstrate the high-performance of our method by simulating a 8×8 RQC with depth $(1 + 25 + 1)$ simply on a personal computer, and a 7×7 circuit with depth $(1 + 40 + 1)$ on the Tianhe-2 [35, 36] supercomputer, which requires only 31 minutes to compute one amplitude with double-precision numbers using 4096 nodes.

Quantum Circuit Simulator Based on PEPS. In the following we consider a two-dimensional rectangular lattice of size $L_v \times L_h$, where L_v and L_h are, respectively, the sizes in the vertical and horizontal directions. We use $N = L_v L_h$ to denote the total number of qubits. The quantum state on such a lattice can be represented as a PEPS [26, 28, 29]

$$|\psi\rangle = \sum_{\sigma_1, \dots, \sigma_N} \mathcal{F}(\mathbf{A}_1^{\sigma_1} \mathbf{A}_2^{\sigma_2} \cdots \mathbf{A}_N^{\sigma_N}) |\sigma_1, \sigma_2, \dots, \sigma_N\rangle, \quad (1)$$

where $\mathbf{A}_n^{\sigma_n}$ is a four dimensional tensor with elements $[\mathbf{A}_n^{\sigma_n}]_{lrud}$ at site n , with $\sigma = 0, 1$ corresponding to the physical dimension, and l, r, u, d corresponding to the left, right, up and down auxiliary dimensions, see Fig. 1(a). The function \mathcal{F} in Eq.(1) indicates the sum over the common auxiliary indices. The bond dimension χ is defined as the maximum size of the four auxiliary dimensions,

$$\chi = \max\{\dim(l), \dim(r), \dim(u), \dim(d)\}, \quad (2)$$

and it characterizes the size of PEPS. For a product quantum state, such as an initialization of a quantum computer to a state with all the qubits set to $|0\rangle$, one has $\chi = 1$ and $|\psi\rangle_{t=0}$ only contains $2N$ complex numbers instead of 2^N .

In the language of PEPS, a single-qubit gate operation on site n only operates locally on the n -th tensor $\mathbf{A}_n^{\sigma_n}$,

and a nearest-neighbour two-qubit gate operation on a pair of sites (n, m) is decomposed into two local operations on the n -th tensor $\mathbf{A}_n^{\sigma_n}$ and the m -th tensor $\mathbf{A}_m^{\sigma_m}$ separately. Thus the cost of each gate operation scales as $O(\chi^4)$ which is negligible for the problems we are tackling. Measuring a single amplitude of the final state $|\psi\rangle$ is done by projecting the $|\psi\rangle$ into a product PEPS with $\chi = 1$, which encodes one spin configuration, and then contracting the resulting tensor network (See Methods for details of the gate operations and measurements on PEPS).

Application to random quantum circuits and complexity analysis. In the following, we apply our PEPS simulator to study the two-dimensional RQC of [37] (see Appendix. A for the details of the circuit). The simulation of this circuit is divided into two parts: (i) circuit evolution and (ii) computing the overlap with randomly selected spin configurations, namely measuring the amplitudes. To quantify the size of the bond dimension required by the tensors, we realize that a single-qubit operation does not affect the size of the tensor it operates on, while a nearest-neighbour two-qubit controlled operation increases the sizes of the two tensors it operates on by a factor of 2 (see Eqs.(10,11) in Methods) [38]. This results in

$$\chi \leq 2^{\lceil d/8 \rceil}, \quad (3)$$

where $\lceil \dots \rceil$ is the ceiling function. The equality in Eq.(3) is reached if the depth d can be divided by 8. Here we point out that since the gate operations on PEPS are numerically cheap, circuit evolution can be performed very efficiently. In fact, we can simulate the exact evolution of a 12×12 lattice to a depth $(1 + 40 + 1)$ within minutes on a personal laptop.

In contrast, a well-known result about PEPS is that performing an exact measurement is an exponentially hard problem [39]. While there exists approximate algorithms for measurements which scale polynomially with χ [27, 30, 31], they are inadequate for random quantum circuits due to the fast growth of entanglement. From now on we ignore both the space and time complexity of circuit evolution and only focus on the measurement, since the cost of the former stage is negligible compared to latter. We also consider that the depth d can be divided by 8 for convenience, which means that each nearest-neighbour pair of qubits are operated on by the same number of two-qubit gate operations, and the size of each auxiliary dimension of each tensor is equal to $\chi = 2^{\lceil d/8 \rceil}$. The process of performing an exact measurement is shown in Fig. 1(b) where the quantum state after the computation is contracted with a product state corresponding to a particular configuration, resulting in a scalar which is the product of N four-dimensional tensors (see Eq.(15) in Methods). Depending on the shape of the lattice, we have developed three different strategies to evaluate this overlap, which are shown in Fig. 2. In Fig.2(a) we show a scheme where the tensor network is contracted row by row (ideal for a thin lattice where,

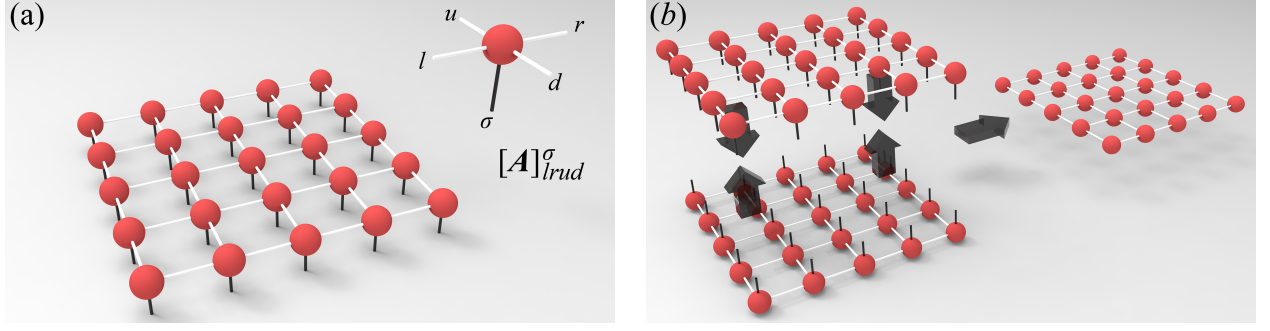


FIG. 1: (a) PEPS on a 5×5 lattice, each qubit of the lattice is represented with a 5 dimensional $[\mathbf{A}]_{l,r,u,d}^\sigma$, where $\sigma = 0, 1$ labels the physical dimension and l, r, u, d label the auxiliary dimensions which connect $[\mathbf{A}]_{l,r,u,d}^\sigma$ to the tensors on the neighbouring sites. (b) Overlapping of two PEPSs by contracting all the physical dimensions of these two PEPSs and all the auxiliary dimensions inside each PEPS.

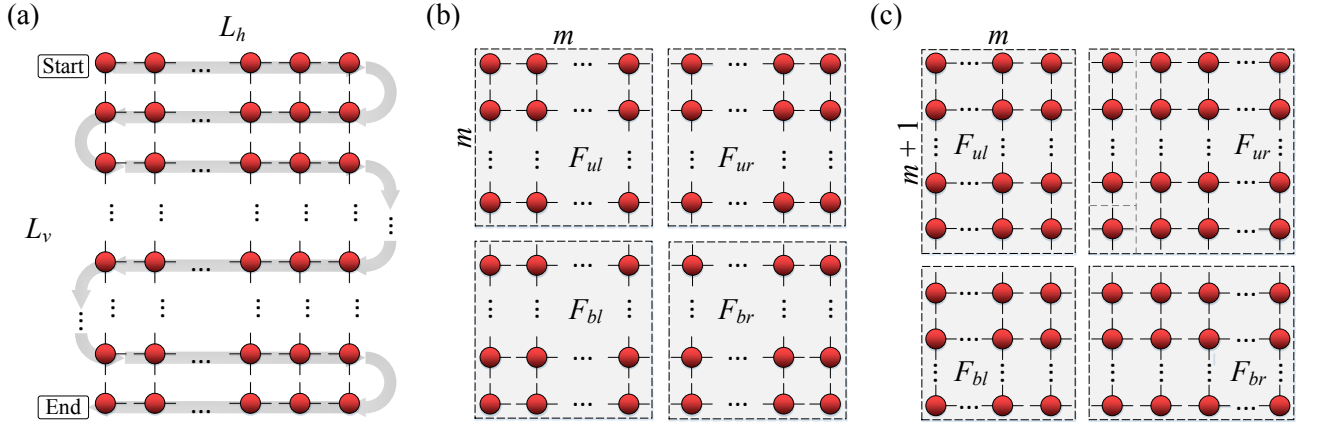


FIG. 2: **Contracting strategies for different lattices.** (a) Generic contracting scheme for lattices with $L_v \geq L_h$. One first contracts the tensors on each horizontal line from top down. For the case with $L_v < L_h$, one can contract the tensors on each vertical lines for left to right. In this strategy, the largest stored tensor is of $\min(L_h, L_v) + 1$ dimension. (b) For a square lattice with an even number of qubits, namely $L_h = L_v = 2m$, the tensor network is divided into four square sub-lattices with sizes $m \times m$. Each sub-lattice is contracted to get a single larger tensor, and then they are contracted to get the probability amplitude. In this strategy, the largest stored tensor has \sqrt{N} indices. (c) For a square lattice with an odd number of qubits, namely $L_h = L_v = 2m + 1$, the tensor network is divided into four sub-lattices, with sizes $(m + 1) \times m$, $(m + 1) \times (m + 1)$, $m \times m$ and $m \times (m + 1)$. The subsequent contraction follows (b), see appendix B for details. In this strategy, the largest stored tensor is of $\sqrt{N} + 1$ dimension.

for instance, $L_v > L_h$). Mathematically, this scheme corresponds to Eqs.(B1-B5) in Appendix. B. The largest tensor involved in this process is $L + 1$ dimensional where we have defined $L = \min(L_h, L_v)$. Assuming a memory efficient implementation of tensor contraction, one would only require a single tensor of such size since the operand tensor could be overwritten. In the mean time, the most time-consuming step is Eq.(B3), in which one contracts two legs of a $L + 1$ dimensional tensor with two legs of another 4-dimensional tensor, a process which is repeated $(L_h - 2)(L_v - 2)$ times. Thus with the contraction scheme in Fig. 2(a), the space and time complexity are

$$\mathcal{C}^s(L_v \times L_h \times d) = 2^{\lceil d/8 \rceil (L+1)}, \quad (4)$$

$$\mathcal{C}^t(L_v \times L_h \times d) = (L_h - 2)(L_v - 2)2^{\lceil d/8 \rceil (L+3)}. \quad (5)$$

Note that these are very accurate evaluations with a clear

prefactor and not just order of magnitude estimates [40].

For the case of a square lattice with an even side length $L_v = L_h = 2m$, a specialized contraction scheme could be used to further reduce the space complexity, which is shown in Fig. 2(b). We first break the lattice into $4m \times m$ blocks. Contracting each block gives us a $2m$ -dimensional tensor, which is then contracted to get the probability amplitude. The largest tensor involved in this process is only $2m$ -dimensional, but at least one additional copy has to be used. In the meantime, the time complexity is determined by the contraction between these $2m$ dimensional tensors, which occurs twice. Thus the space and

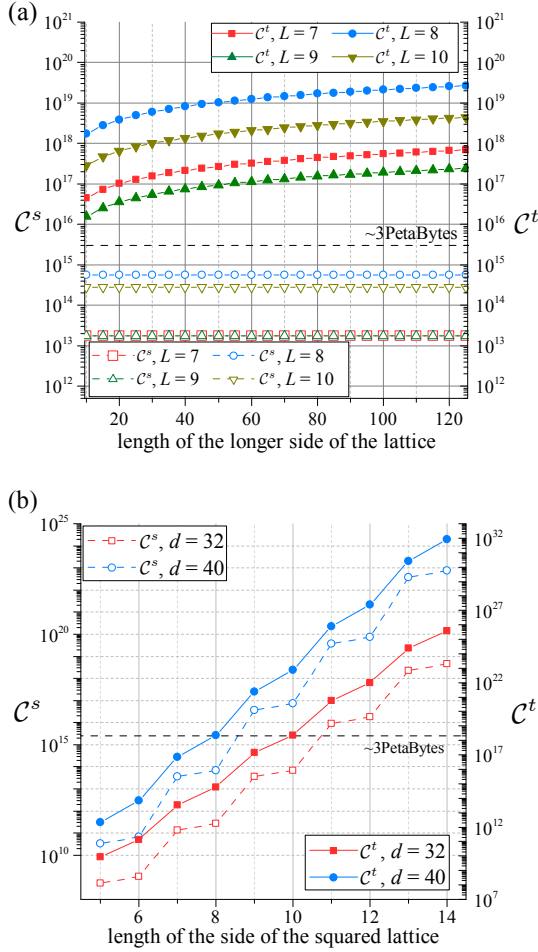


FIG. 3: The space and time complexity of RQCs based on the PEPS quantum circuit simulator. The solid lines in both figures correspond to the time complexity \mathcal{C}_t and the dashed lines correspond to the space complexity \mathcal{C}_s . The grey dotted line represents the current memory limit of supercomputers (2.17PB for Tianhe-2 and 2.67 PB for summit). (a) Scaling of space and time complexity with the longer side of rectangular lattices. Lines with different colours correspond to different minimum lateral dimensions L . The depth $d = 1 + 40 + 1$ for lines with $L = 7, 8$, and $d = 1 + 32 + 1$ for lines with $L = 9, 10$. (b) Theoretical space and time complexity for square lattices with different sizes. Lines with different colours correspond to different circuit depths.

time complexity become

$$\mathcal{C}^s(2m \times 2m \times d) = 2^{(\lceil d/8 \rceil \sqrt{N})+1}, \quad (6)$$

$$\mathcal{C}^t(2m \times 2m \times d) = 2^{(3\lceil d/8 \rceil \sqrt{N}/2)+1}. \quad (7)$$

Compared to Eq.(4), the space complexity is reduced by a factor $\chi/2$, which means that for $d = 40$ one requires 16 times less memory. However the time complexity is larger by a factor $\chi^{\sqrt{N}/2}/[(L_h - 2)(L_v - 2)]$.

For a square lattice with odd side length $L_v = L_h = 2m + 1$, as for the 7×7 case studied later, we propose to use Fig. 2(c) to compute one amplitude. In this case

one needs to store, at most, a single $2m + 2$ -dimensional tensor, plus a $2m + 1$ -dimensional tensor. The time cost mainly comes from a multiplication of a $2m + 2$ dimensional tensor with a $2m + 1$ dimensional tensor, and a multiplication of a $2m + 1$ dimensional tensor with a $2m$ dimensional tensor (Our actual implementation is slightly different from this and has a slightly higher time complexity, see Appendix. B for more detail). Thus the space and time complexity are

$$\mathcal{C}^s((2m + 1) \times (2m + 1) \times d) = 2^{\lceil d/8 \rceil (\sqrt{N}+1)} + 2^{\lceil d/8 \rceil \sqrt{N}}, \quad (8)$$

$$\mathcal{C}^t((2m + 1) \times (2m + 1) \times d) = (2^{\lceil d/8 \rceil} + 1)2^{\lceil d/8 \rceil (3\sqrt{N}-1)/2}. \quad (9)$$

We point out here that although Eq.(9) has higher time complexity compared to Eq.(5), it can be more conveniently parallelized when executed on a supercomputer because it avoids massive data transfer. Therefore we implement the schemes of Fig. 2(b,c) for more demanding calculations. In Fig.3(a) we show the space and time complexities for $8 \times l$ circuits for $d = 1 + 40 + 1$ (or $10 \times l$ circuits with depth of $d = 1 + 32 + 1$), showing that they are within reach for state-of-the-art supercomputers. This shows clearly where the frontier for quantum supremacy stands for this random quantum circuit and for our method. In Fig.3(b) we show the space and time complexities computed from Eqs.(6-9). To this end, we note that our algorithm can be straightforwardly combined with the fast sampling technique in [24] to measure a large number of amplitudes. Following Fig. 2(b), one can sample in the region F_{bl} with negligible additional cost since the regions F_{ul} , F_{ur} and F_{br} can be reused.

To give more precise numbers, simulating a 8×8 lattice to a depth $(1+40+1)$ (same space complexity of a 10×10 circuit to a depth $(1+32+1)$), it would require, from Eq.(6), 32 TB of memory, while simulating a $8 \times l$ (with $l > 8$) lattice to a depth $(1+40+1)$ would require about 0.5 PB memory. In contrast, simulating a 9×9 lattice with a depth 40 would require 16 PB (petabytes) memory and simulating a 12×12 lattice to a depth $(1+32+1)$ would require 8 PB memory, which are currently out of reach. Our circuit simulator can straightforwardly be extended to other types of two-dimensional lattices including Google Bristlecone QPU architecture. By applying a complexity analysis to this architecture, we find that it only requires less than a manageable 0.6 PB of memory to simulate an RQC with 72 qubits at depth $(1+32+1)$ (details of the analysis are in the Appendix. C).

As a first test we have implemented small scale simulations on a personal computer, which takes less than 1 hour to measure one amplitude of a 8×8 circuit to a depth $(1+25+1)$ with 100% fidelity. We have measured 10000 random samples on a 24-core workstation, using 1 thread for each simulation, and obtained the Porter-Thomas distribution with high accuracy (see Appendix. B for more details).

Massive Parallel Benchmarking on Supercom-

TABLE I: **Benchmarking PEPS based circuit simulator.** Results from previous groups are listed (with Year and Reference) and the Platform used. The simulation scale is shown in the form of “Qubits \times Depth”. The column denoted by “Node Usage” indicates the number of cores used divided by the total available cores of the computing platform, and the corresponding percentage. The theoretical peak performance and the total memory of the used computing nodes are listed in columns denoted by $R_{\text{Node-peak}}$ and Mem_{Node} . The elapsed time for the simulation is listed in the last column. Below the dotted line we list the performance of our simulator executed on Tianhe-2 with double-precision numbers. The performance the theoretical peak performance of Tianhe-2 nodes only consists of the performance of CPUs, and that of the accelerators are not taken into account. We note that in the RQC originally proposed in [3], the instances in which a T gate follows a CZ gate can be exploited to reduce the computational cost, as is done for example in [20, 21]. This weakness has been later removed in the prescription for RQC detailed in [24] which we follow.

Year/Ref.	Simulation Scale	Platform	Node Usage	$R_{\text{Node-peak}}$	Mem_{Node}	Elapsed Time
2017[19]	$5 \times 9 \times (1 + 25 + 1)$	Cori II	8,192/9,304, 88%	24.6PFlops	0.74PB	10 min
2017[41]	$7 \times 7 \times (1 + 27 + 1)$	Vulcan	4,096/24,576, 16%	0.84PFlops	0.06PB	2 d
2018[21, 42]	$7 \times 7 \times (1 + 39 + 1)$	Sunway TaihuLight	32,768/40,960, 80%	100.3PFlops	1.00PB	4.2 hr
.....
	$7 \times 7 \times (1 + 39 + 1)$		4,096/17,920, 22%	1.73PFlops	0.50PB	9 min
	$7 \times 7 \times (1 + 40 + 1)$		4,096/17,920, 22%	1.73PFlops	0.50PB	31 min
2019	$8 \times 8 \times (1 + 37 + 1)$	Tianhe-2	4,096/17,920, 22%	1.73PFlops	0.50PB	68 min
	$9 \times 9 \times (1 + 31 + 1)$		2,048/17,920, 11%	0.87PFlops	0.25PB	22 min
	$10 \times 10 \times (1 + 26 + 1)$		1,024/17,920, 5%	0.43PFlops	0.13PB	9 min

puter. We have implemented our large scale tensor contraction algorithms based on an open-source software package Cyclops Tensor Framework [43], with MPI and OpenMP as the parallel interfaces. The massive parallel benchmarking was then executed on Tianhe-2 supercomputer. According to the features of the supercomputer platform and the results of the scaling test, we chose to use one MPI process with 24 OpenMP threads on each node. Each normal node contains two 12-core CPUs, and is equipped with 64GB (128 GB on each fat node) memory. The maximum number of nodes used reaches 4,096 (98,304 compute cores in total), which is less than 1/4 of the whole system, and since we only use CPUs, the peak performance we use is ~ 1.73 PFlops. All our calculations are done with double-precision numbers. Our results are listed in table I and compared to state-of-the-art calculations on square and rectangular RQC with unit fidelity [44].

The calculation with the largest number of qubits is a 10×10 circuit with $d = (1 + 26 + 1)$, which is done on 1,024 normal nodes and takes 6 minutes to measure one amplitude, following the contraction strategy in Fig. 2(b). The calculation with the largest depth is a 7×7 circuit with $d = (1 + 40 + 1)$, which is done on 4,096 fat nodes and takes 31 minutes. On each fat node 23.13 GB memory is used, and thus this simulation takes 92.51 TB memory in total. To pursue efficiency, parts of the data is duplicated on several computing nodes to reduce the cost of data communication, leading to a larger memory usage than theoretical prediction 16 TB. When comparing to other methods and platforms, the PEPS simulator performance stands out, see Table. I.

Conclusion. In this work we have adapted the Projected Entangled-Pair States algorithm from many-body quantum physics to build a general-purpose quantum cir-

cuit simulator. With this circuit simulator, we have computed the exact complexity analysis of a standard random quantum circuit [37]. Based on this analysis, we point out that simulating an $8 \times l$ to a depth $(1 + 40 + 1)$ or Bristlecone-72 circuit to a depth $(1 + 32 + 1)$ are within reach of current supercomputing platforms. With the exact thresholds for complexity, it is possible to evaluate the size and depth of random quantum circuits that can be computed classically when more powerful supercomputers become available in the future. Hence we have a clear way to determine where the quantum supremacy frontier stands for this type of problems.

We highlight that we have presented a general-purpose quantum circuit simulator which can be readily used to compute generic algorithms implementable on 2D platforms. Since it produces the full wave function, it can readily be used for projective measurements, to compute average values of observables and sequences of measurements.

We have implemented numerical experiments on a personal computer with a 8×8 circuit to a depth $(1 + 25 + 1)$, and with Tianhe-2 supercomputer with a 10×10 circuit to a depth $(1 + 26 + 1)$, as well as a 7×7 circuit to a depth $(1 + 40 + 1)$, and compared them to recent works from other groups. Currently our results have 100% fidelity with the exact wave function, however we could also investigate the trade-off between fidelity and speed, so as to be able to sample many trajectories. This investigation is left for future works, together with the plan to include the effects of noise or errors in order to characterize more closely the actual behavior of a noisy intermediate-scale quantum computer.

Acknowledgments

We gratefully acknowledge the help from China Great-wall Technology and National Supercomputing Center in Guangzhou. C. G. acknowledges support from National Natural Science Foundation of China under Grants No.

11504430 and No. 11805279. D.P. acknowledges support from the Singapore Ministry of Education, Singapore Academic Research Fund Tier-II (project MOE2016-T2-1-065). J.W. acknowledges support from National Natural Science Foundation of China under Grants No. 61632021.

-
- [1] Richard P Feynman. Simulating physics with computers. *International journal of theoretical physics*, 21(6):467–488, 1982.
 - [2] Peter W Shor. Algorithms for quantum computation: Discrete logarithms and factoring. In *Proceedings 35th annual symposium on foundations of computer science*, pages 124–134. Ieee, 1994.
 - [3] Sergio Boixo, Sergei V Isakov, Vadim N Smelyanskiy, Ryan Babbush, Nan Ding, Zhang Jiang, Michael J Bremner, John M Martinis, and Hartmut Neven. Characterizing quantum supremacy in near-term devices. *Nature Physics*, 14(6):595, 2018.
 - [4] AP Lund, Michael J Bremner, and TC Ralph. Quantum sampling problems, bosonsampling and quantum supremacy. *npj Quantum Information*, 3(1):15, 2017.
 - [5] He-Liang Huang, Qi Zhao, Xiongfeng Ma, Chang Liu, Zu-En Su, Xi-Lin Wang, Li Li, Nai-Le Liu, Barry C Sanders, Chao-Yang Lu, et al. Experimental blind quantum computing for a classical client. *Physical review letters*, 119(5):050503, 2017.
 - [6] Jiehang Zhang, Guido Pagano, Paul W Hess, Antonis Kyprianidis, Patrick Becker, Harvey Kaplan, Alexey V Gorshkov, Z-X Gong, and Christopher Monroe. Observation of a many-body dynamical phase transition with a 53-qubit quantum simulator. *Nature*, 551(7682):601, 2017.
 - [7] He-Liang Huang, Xi-Lin Wang, Peter P Rohde, Yi-Han Luo, You-Wei Zhao, Chang Liu, Li Li, Nai-Le Liu, Chao-Yang Lu, and Jian-Wei Pan. Demonstration of topological data analysis on a quantum processor. *Optica*, 5(2):193–198, 2018.
 - [8] K Wright, KM Beck, S Debnath, JM Amini, Y Nam, N Grzesiak, J-S Chen, NC Pienti, M Chmielewski, C Collins, et al. Benchmarking an 11-qubit quantum computer. *arXiv preprint arXiv:1903.08181*, 2019.
 - [9] Julian Kelly, Zijun Chen, Ben Chiaro, Brooks Foxen, John Martinis, and Quantum Hardware Team Team. Operating and characterizing of a 72 superconducting qubit processor “bristlecone”: Part 1. In *APS Meeting Abstracts*, 2019.
 - [10] Ming Gong, Ming-Cheng Chen, Yarui Zheng, Shiyu Wang, Chen Zha, Hui Deng, Zhiguang Yan, Hao Rong, Yulin Wu, Shaowei Li, et al. Genuine 12-qubit entanglement on a superconducting quantum processor. *Physical Review Letters*, 122(11):110501, 2019.
 - [11] Xi-Lin Wang, Yi-Han Luo, He-Liang Huang, Ming-Cheng Chen, Zu-En Su, Chang Liu, Chao Chen, Wei Li, Yu-Qiang Fang, Xiao Jiang, et al. 18-qubit entanglement with six photons three degrees of freedom. *Physical review letters*, 120(26):260502, 2018.
 - [12] John Preskill. Quantum computing and the entanglement frontier. *arXiv preprint arXiv:1203.5813*, 2012.
 - [13] Scott Aaronson and Alex Arkhipov. The computational complexity of linear optics. In *Proceedings of the forty-third annual ACM symposium on Theory of computing*, pages 333–342. ACM, 2011.
 - [14] Junjie Wu, Yong Liu, Baida Zhang, Xianmin Jin, Yang Wang, Huiquan Wang, and Xuejun Yang. A benchmark test of boson sampling on Tianhe-2 supercomputer. *National Science Review*, 5(5):715–720, 2018.
 - [15] Dan Shepherd and Michael J Bremner. Temporally unstructured quantum computation. *Proceedings of the Royal Society A: Mathematical, Physical and Engineering Sciences*, 465(2105):1413–1439, 2009.
 - [16] Michael J Bremner, Richard Jozsa, and Dan J Shepherd. Classical simulation of commuting quantum computations implies collapse of the polynomial hierarchy. *Proceedings of the Royal Society A: Mathematical, Physical and Engineering Sciences*, 467(2126):459–472, 2010.
 - [17] Adam Bouland, Bill Fefferman, Chinmay Nirkhe, and Umesh Vazirani. Quantum supremacy and the complexity of random circuit sampling. *arXiv preprint arXiv:1803.04402*, 2018.
 - [18] Sergio Boixo, Sergei V Isakov, Vadim N Smelyanskiy, and Hartmut Neven. Simulation of low-depth quantum circuits as complex undirected graphical models. *arXiv preprint arXiv:1712.05384*, 2017.
 - [19] Thomas Häner and Damian S Steiger. 0.5 petabyte simulation of a 45-qubit quantum circuit. In *Proceedings of the International Conference for High Performance Computing, Networking, Storage and Analysis*, page 33. ACM, 2017.
 - [20] Zhao-Yun Chen, Qi Zhou, Cheng Xue, Xia Yang, Guangcan Guo, and Guo-Ping Guo. 64-qubit quantum circuit simulation. *Science Bulletin*, 63(15):964–971, 2018.
 - [21] Riling Li, Bujiao Wu, Mingsheng Ying, Xiaoming Sun, and Guangwen Yang. Quantum supremacy circuit simulation on sunway taihulight. *arXiv preprint arXiv:1804.04797*, 2018.
 - [22] Ming-Cheng Chen, Riling Li, Lin Gan, Xiaobo Zhu, Guangwen Yang, Chao-Yang Lu, and Jian-Wei Pan. Quantum teleportation-inspired algorithm for sampling large random quantum circuits. *arXiv preprint arXiv:1901.05003*, 2019.
 - [23] Sergei V. Isakov Sergio Boixo Igor L. Markov, Aneeqa Fatima. Quantum supremacy is both closer and farther than it appears. *arXiv preprint arXiv:1807.10749*, 2018.
 - [24] Benjamin Villalonga, Sergio Boixo, Bron Nelson, Christopher Henze, Eleanor Rieffel, Rupak Biswas, and Salvatore Mandrà. A flexible high-performance simulator for the verification and benchmarking of quantum circuits implemented on real hardware. *arXiv preprint arXiv:1811.09599*, 2018.
 - [25] Benjamin Villalonga, Dmitry Lyakh, Sergio Boixo, Hartmut Neven, Travis S Humble, Rupak Biswas, Eleanor G Rieffel, Alan Ho, and Salvatore Mandrà. Establishing the

- quantum supremacy frontier with a 281 pflop/s simulation. *arXiv preprint arXiv:1905.00444*, 2019.
- [26] Frank Verstraete and J Ignacio Cirac. Renormalization algorithms for quantum-many body systems in two and higher dimensions. *arXiv preprint cond-mat/0407066*, 2004.
- [27] Frank Verstraete, Michael M Wolf, David Perez-Garcia, and J Ignacio Cirac. Criticality, the area law, and the computational power of projected entangled pair states. *Physical review letters*, 96(22):220601, 2006.
- [28] Valentin Murg, Frank Verstraete, and J Ignacio Cirac. Variational study of hard-core bosons in a two-dimensional optical lattice using projected entangled pair states. *Physical Review A*, 75(3):033605, 2007.
- [29] Jacob Jordan, Roman Orús, Guifre Vidal, Frank Verstraete, and J Ignacio Cirac. Classical simulation of infinite-size quantum lattice systems in two spatial dimensions. *Physical review letters*, 101(25):250602, 2008.
- [30] Zheng-Cheng Gu, Michael Levin, and Xiao-Gang Wen. Tensor-entanglement renormalization group approach as a unified method for symmetry breaking and topological phase transitions. *Physical Review B*, 78(20):205116, 2008.
- [31] Hong-Chen Jiang, Zheng-Yu Weng, and Tao Xiang. Accurate determination of tensor network state of quantum lattice models in two dimensions. *Physical review letters*, 101(9):090603, 2008.
- [32] Zhi-Yuan Xie, Hong-Chen Jiang, Qunjun N Chen, Zheng-Yu Weng, and Tao Xiang. Second renormalization of tensor-network states. *Physical review letters*, 103(16):160601, 2009.
- [33] Valentin Murg, Frank Verstraete, and J Ignacio Cirac. Exploring frustrated spin systems using projected entangled pair states. *Physical Review B*, 79(19):195119, 2009.
- [34] Román Orús. A practical introduction to tensor networks: Matrix product states and projected entangled pair states. *Annals of Physics*, 349:117–158, 2014.
- [35] Xiangke Liao, Liquan Xiao, Canqun Yang, and Yutong Lu. MilkyWay-2 supercomputer: system and application. *Frontiers of Computer Science*, 8(3):345–356, 2014.
- [36] Xiangke Liao. MilkyWay-2: back to the world Top 1. *Frontiers of Computer Science*, 8(3):343–344, 2014.
- [37] Available on github at <https://github.com/sboixo/grcs>.
- [38] If an iswap gate is used instead of a cz gate, then the size of the two tensors it acts on will increase by a factor 4, effectively halving the depth of the circuit that can be simulated.
- [39] Norbert Schuch, Michael M Wolf, Frank Verstraete, and J Ignacio Cirac. Computational complexity of projected entangled pair states. *Physical review letters*, 98(14):140506, 2007.
- [40] The time complexity can be reduced by using advanced matrix-matrix multiplications schemes and by parallelizing the operation.
- [41] Edwin Pednault, John A Gunnels, Giacomo Nannicini, Lior Horeh, Thomas Magerlein, Edgar Solomonik, and Robert Wisnieff. Breaking the 49-qubit barrier in the simulation of quantum circuits. *arXiv preprint arXiv:1710.05867*, 2017.
- [42] In [21] the authors also compute an instance for a 7×7 ($1+55+1$) random quantum circuit, which is however especially designed to calculate a single amplitude and not easily scalable to calculate a large number of amplitudes.
- [43] Edgar Solomonik, Devin Matthews, Jeff R Hammond, John F Stanton, and James Demmel. A massively parallel tensor contraction framework for coupled-cluster computations. *Journal of Parallel and Distributed Computing*, 74(12):3176–3190, 2014.
- [44] In [25] the authors compute, with 0.5% fidelity, 10^6 amplitudes for a 7×7 ($1+40+1$) random quantum circuit with single-precision numbers on Summit in 2.4 hours, using 2.67 PB memory and $R_{peak} = 200.8$ PFlops.

Methods.

Gate Operation A single-qubit gate U_σ^τ acting on n -th qubit of the lattice can be written as

$$[\mathbf{A}'_n{}^{\tau_n}]_{lrud} = \sum_{\sigma} U_{\sigma_n}^{\tau_n} [\mathbf{A}_n^{\sigma_n}]_{lrud}. \quad (10)$$

As we can see from Eq.(10), the size of the local tensor is not affected by a single-qubit gate operation. For a two-qubit gate acting on a vertically nearest-neighbour pair of qubits (n, m) , denoted as $O_{\sigma_n, \sigma_m}^{\tau_n, \tau_m}$, we first use a singular value decomposition (SVD) to factorize it into a product of two local tensors

$$\text{SVD}(O_{\sigma_n, \sigma_m}^{\tau_n, \tau_m}) = \sum_s U_{\sigma_n, s}^{\tau_n} V_{s, \sigma_m}^{\tau_m}, \quad (11)$$

where the singular values have been absorbed into U as $U_{\sigma_n, s}^{\tau_n} := \sum_s U_{\sigma_n, s}^{\tau_n} S_{s, s}$. The size of the auxiliary dimension s is denoted as χ_o , which, for any two-qubit controlled gate, is $\chi_o = 2$. The two local tensors U and V are then applied the two qubits n and m separately, as for a single-qubit gate operation,

$$[\mathbf{A}'_n{}^{\tau_n}]_{lrud'} = \sum_{\sigma_n} U_{\sigma_n, s}^{\tau_n} [\mathbf{A}_n^{\sigma_n}]_{lrud}, \quad (12)$$

$$[\mathbf{A}'_m{}^{\tau_m}]_{lru'd} = \sum_{\sigma_m} V_{s, \sigma_m}^{\tau_m} [\mathbf{A}_j^{\sigma_m}]_{lrud}. \quad (13)$$

Here we have used the indices $d' = (d, s)$, $u' = (s, u)$, which bundles the two tensor dimensions into one. As a result, χ increases by a factor of χ_o . To keep χ in a affordable size, one would usually use a subsequent singular value decomposition to compress the resulting tensors by throwing away singular values below certain threshold. However, we point out that for random quantum circuits we cannot perform such a compression because the distribution of the singular values after the two-qubit gate operation is almost flat, making it impossible for compression (this is also an indication that this problem has large bipartite entanglement across the whole circuit). Moreover, random quantum circuits are extremely sensitive to errors, thus small truncation error could possibly change significantly the sampling distribution.

Measurement To extract information from PEPS, one needs to perform measurements on it, and this is by far the most challenging step. Since our algorithms is generic, it allows both projective measurements and direct computation of average values, although we only need the first one for the discussion in the manuscript.

To perform the projection of the wave function onto a given computational basis element $|\vec{\tau}\rangle$ we first write this

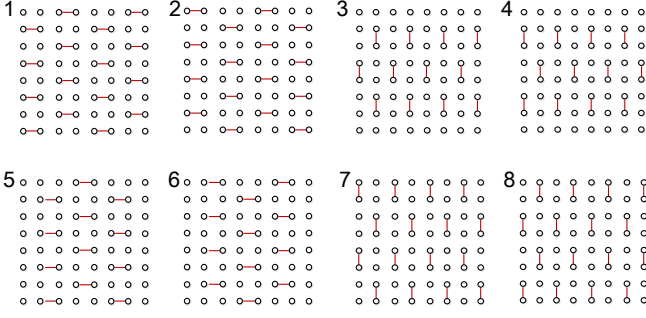


FIG. 4: Layout of the CZ gates for the two-dimensional random quantum circuit.

basis element as a product PEPS (i.e. $\chi = 1$)

$$|\vec{\tau}\rangle = |\tau_1, \tau_2, \dots, \tau_N\rangle. \quad (14)$$

Then we contract all the physical indexes of $|\psi\rangle$ with that of $|\tau\rangle$, which results in a new two dimensional lattice made of $L_v \times L_h$ four dimensional tensors $[\mathbf{E}_n]_{lrud} = [\mathbf{A}_n^{\sigma_n = \tau_n}]_{lrud}$. As a result, we have

$$\langle \vec{\tau} | \psi \rangle = \mathcal{F}(\mathbf{E}_1 \mathbf{E}_2 \cdots \mathbf{E}_N). \quad (15)$$

This process is graphically shown in Fig. 1(b). We can see that the auxillary dimensions of \mathbf{E}_n remains the same as that of $\mathbf{A}_n^{\sigma_n}$, which we still denote as χ . Evaluating Eq.(15) exactly requires to contract the whole tensor network, which is known to be a difficult problem [26, 34]. The details to evaluate Eq.(15) exactly are shown in Appendix A.

We now present briefly how to compute the expectation value of a given observable. Here we only consider the simple case that the observable is local and represented as a 2×2 matrix \hat{O} . We first apply \hat{O} onto the state $|\psi\rangle$ in the same way as a single-qubit gate operation as in Eq.(10). Then we compute the overlap with $\langle \psi |$ using Eq.(15) and get

$$\bar{O} = \langle \psi | \hat{O} | \psi \rangle. \quad (16)$$

Unlike projective measurements, the resulting tensor network has a bond dimension χ^2 .

Appendix A: Introduction to Random Quantum Circuits

For a $L_v \times L_h$ qubit lattice, the Random Quantum Circuit is defined as follows (see Fig. 4):

1. Apply a Hadamard gate to each qubit to initialize the qubits to a symmetric superposition.
2. Apply controlled-phase (CZ) gates alternating between eight configurations similar to Fig. 4 to entangle neighbouring qubits.
3. Apply a randomly chosen gate (T, $X^{1/2}$ or $Y^{1/2}$) to each qubit on which the CZ gates has not just been applied, according to the rules in [3].

4. Repeat steps 2 and 3 to add layers of depth to the circuit.

5. Apply a final Hadamard gate to each qubit.

It has been proven that this random quantum circuit satisfies both average-case hardness and anti-concentration condition [17], and hence it cannot be efficiently simulated on a classical computer.

Appendix B: Algorithm for Exact Computation of the Overlap

In the following we show a generic way to evaluate Eq.(15) exactly. Assuming $L_h \leq L_v$, we first contract all the tensors on the first row to get a L_h dimensional tensor

$$F_1^{d_{(1,1)}, d_{(1,2)}, \dots, d_{(1, L_h)}} = \mathcal{F} \left([\mathbf{E}_{(1,1)}]_{d_{(1,1)}} \cdots [\mathbf{E}_{(1, L_h)}]_{d_{(1, L_h)}} \right), \quad (B1)$$

where the bottom legs $d_{(1,n)}$ of $\mathbf{E}_{(1,n)}$ ($1 \leq i \leq L_h$) are written explicitly to indicate that they are not contracted in this step. Note also the notation for the position with two numbers instead of one, i.e. (n, m) indicates the qubit on the n -th row and m -th column. Next we contract F_1 with the first tensor in the second row $\mathbf{E}_{(2,1)}$ and get

$$G_1^{r_{(2,1)}, d_{(2,1)}, d_{(1,2)}, \dots, d_{(1, L_h)}} = \sum_{d_{(1,1)}} F_1^{d_{(1,1)}, \dots, d_{(1, L_h)}} \times [\mathbf{E}_{(2,1)}]_{r_{(2,1)} d_{(1,1)} d_{(2,1)}}, \quad (B2)$$

where we have used the fact that for \mathbf{E}_{21} one has the size $\dim(l_{(2,1)}) = 1$ and $u_{(2,1)} = d_{(1,1)}$. The resulting tensor G_1 is a $L_h + 1$ dimensional tensor. Then we contract G_1 with the second tensor in the second row $\mathbf{E}_{(2,2)}$ and get

$$G_2^{r_{(2,2)}, d_{(2,1)}, d_{(2,2)}, \dots, d_{(1, L_h)}} = \sum_{r_{(2,1)}, d_{(1,2)}} G_1^{r_{(2,1)}, d_{(2,1)}, d_{(1,2)}, \dots, d_{(1, L_h)}} [\mathbf{E}_{22}]_{r_{(2,1)} r_{(2,2)} d_{(1,2)} d_{(2,2)}}, \quad (B3)$$

where we have used the fact that for $\mathbf{E}_{(2,2)}$ one has $l_{(2,2)} = r_{(2,1)}$ and $u_{(2,2)} = d_{(1,2)}$, and the resulting tensor G_2 is again a $L_h + 1$ dimensional tensor. We can repeat this procedure and move on to the right until we have contracted all the tensors on the second row and get

$$F_2^{d_{(2,1)}, d_{(2,2)}, \dots, d_{(2, L_h)}} = G_{L_h}^{r_{(2, L_h)}, d_{(2,1)}, d_{(2,2)}, \dots, d_{(2, L_h)}} \quad (B4)$$

where we have used the fact $\dim(r_{(2, L_h)}) = 1$ and redefined G_{L_h} and F_2 . Noticing that F_2 has the same structure as F_1 , therefore we repeat this procedure until we have reached the last row and get F_L , which is a scalar since all the indexes $\dim(d_{(L_v, n)}) = 1$ for $1 \leq n \leq L_h$. Thus we get

$$\langle \vec{\tau} | \psi \rangle = F_L. \quad (B5)$$

From this analysis it appears that the largest tensor involved in this procedure is $L_h + 1$ dimensional. Moreover, for $L_h > L_v$, instead of moving from top down, it is straightforward to slightly modify the algorithm to move from left to right, and the largest tensor involved would become $L_v + 1$ dimensional. Therefore the memory required scales exponentially with the exponent $\min(L_h + 1, L_v + 1)$.

For the special case of a square lattice with $L_h = L_v = \sqrt{N}$, it is possible to improve the performance via a particular partitioning of the sum. The partitioning strategies for network with even or odd side length are different, as shown in Fig. 2(b,c) respectively. For the network with even side lengths, tensors are divided into four parts first, as Fig. 2(b) illustrates. We start the contraction of the tensors from the upper-left partition, obtaining a tensor with dimension \sqrt{N} which we refer to as F_{ul} . Similarly, the other three partitions produce another three \sqrt{N} dimension tensors, denoted as F_{ur} (upper-right), F_{bl} (bottom-left) and F_{br} (bottom-right). Then, we contract F_{ul} with F_{ur} , and F_{bl} with F_{br} . Consequently, by contracting the remaining two tensors together, we get the amplitude value.

The algorithm for the network with odd side lengths ($L_h = L_v = 2m + 1$) is relatively more complicated. The tensors are partitioned into 4 groups, as shown in Fig. 2(c). The contraction starts from the up-left $(m + 1) \times m$ partition, producing a \sqrt{N} dimension tensor denoted as F_{ul} . Then we move to the other three parts and contract them into F_{ur}, F_{bl}, F_{br} same as F_{ul} . The contraction of F_{ur} can again be divided into 4 sub-procedures, which are indicated in Fig. 2(c) by the gray dashed lines that break the lattices into 3 small groups. The sub-procedures are: (1) Contracting the right $(m + 1) \times m$ tensors into a \sqrt{N} -dimension tensor; (2) Contracting the first m tensors at the $m + 1$ -th column into a \sqrt{N} -dimension tensor; (3) Contracting the two \sqrt{N} -dimension tensors from procedure (1) and (2) into a $(\sqrt{N} + 1)$ -dimension tensor; (4) Contracting the obtained $(\sqrt{N} + 1)$ -dimension tensor with the 4-dimension tensor located in the center of the lattice (which is also the left-bottom corner of F_{ur}), and resulting in a $(\sqrt{N} + 1)$ -dimensional tensor. Then, by contracting the four parts together, we get the probability amplitude. We note that the time complexity of this implementation is

$$\mathcal{C}^t((2m + 1) \times (2m + 1) \times d) = 2^{\lceil d/8 \rceil (3\sqrt{N} + 1)/2 + 1}. \quad (\text{B6})$$

We compute the projection over 10000 randomly chosen configurations for an 8×8 circuit with depth $(1 + 25 + 1)$. We can then plot the frequency with which each probability of configurations appear. This is represented in Fig. 5 by blue circles while the red continuous line shows the Porter-Thomas distribution, which is what is expected theoretically.

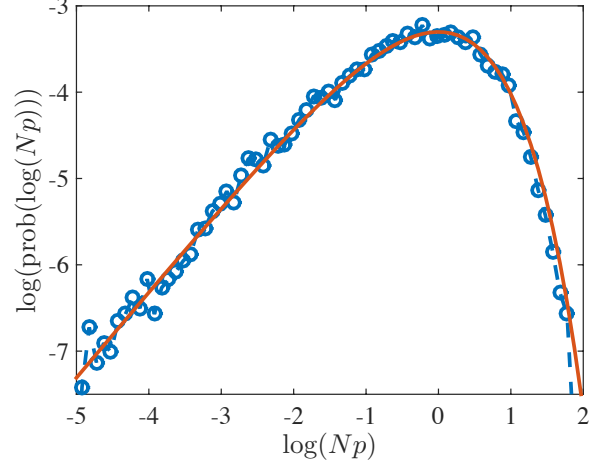


FIG. 5: The blue circles show the log transformed probabilities from 10000 measurement outcomes, while the red line is the log transformed Porter-Thomas distribution. The circuit size is 8×8 with a depth $(1 + 25 + 1)$.

Appendix C: Complexity Analysis of Google Bristlecone QPU

To simulate the Google Bristlecone QPU with PEPS, both the representation of the quantum state as well as the gate operations are implemented exactly in the same way as for the rectangular lattice case. The only difference is that during the measurement stage, the tensor network that needs to be contracted are rotated by 45 degree compared to a rectangular lattice. In Fig. 6 we show a contraction strategy for the simulation of a Google Bristlecone QPU. From Fig. 6 we can see that the number of legs of a tensor is at most 11, and hence the space cost for simulating this circuit to a depth $(1 + 32 + 1)$ with our circuit simulator scales as $2^{32/8 \times 11 + 1} = 2^{45}$, which corresponds to less than 0.6 PB memory.

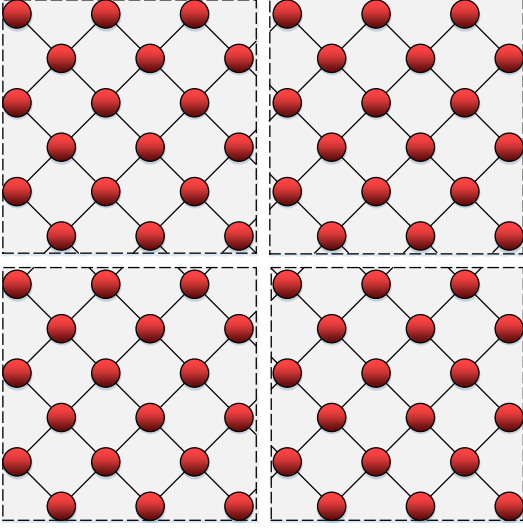


FIG. 6: Contracting strategy for the Google Bristlecone QPU. The 12×6 lattice is partitioned into four sub-lattices with size 6×3 . Contracting all the sub-lattices would result in 4 large tensors with ranks 11, 10, 10, 11 (which can be seen by counting the legs which are not contracted.) respectively. Contracting these 4 large tensors would require to store at least two 11-dimensional tensors.